GNC Robustness Stability Verification for an Autonomous Lander

GNC Robustness Stability Verification for an Autonomous Lander

Michele Pagone[a, *, 1]; Carlo Novara[a, 2]; Paolo Martella[b, 3]; Claudio Nocerino[b, 4]

[a] *Department of Electronics and Telecommunication, Politecnico di Torino, Corso Duca degli Abruzzi, 24, 10129, Torino, Italy,*

[b] *Thales Alenia Space Italy, Strada Antica di Collegno, 253, 10146, Torino, Italy,*

*Corresponding Author

[1] Ph.D. Fellow, Department of Electronics and Telecommunications, Politecnico di Torino, *michele.pagone@polito.it*.

[2] Professor, Department of Electronics and Telecommunications, Politecnico di Torino, *carlo.novara@polito.it*.

[3] GNC Engineer, Thales Alenia Space Italy, *Paolo.Martella@thalesaleniaspace.com*.

[4] GNC Engineer, Thales Alenia Space Italy, *claudio.nocerino@thalesaleniaspace.com*.

Abstract

In the context of Solar System exploration, autonomous planetary surface missions represent, nowadays, an important step in scientific research. Nevertheless, the design of landing Guidance, Navigation and Control sub-systems is one of the most challenging and complex tasks. Indeed, during the propelled landing phase, the system must be controlled in closed-loop, ensuring the stability of the lander motion with a certain level of robustness. This paper proposes a novel procedure for the verification of the lander nominal and robust stability. The first step is to perform a model simplification, in order to reduce the involved degrees of freedom and allow a decoupled analysis of the rotational and translational dynamics. Then, the classical stability theorems are applied, taking also into account the uncertainties due to actuators and sensors. Next, a robustness stability verification is performed by means of μ-Analysis. Finally, a Monte Carlo campaign is carried out, using an End-to-End simulator in order to verify, in the time domain, the reliability of the analytical stability analysis. The procedure is applied to a case study representing a descent module during the controlled landing phase on the Mars surface.

Keywords: *Landing; Control; Stability; Robustness; Monte Carlo; μ-Analysis.*

Notation

The bold type is referred to vectors and the capital bold type is referred to matrices, where not differently specified. Force and Torque vectors are represented with a capital bold type.

θ: Off-Vertical Angle

$v = [v_x, v_y, v_z]^T$: Velocity

$\omega = [\omega_x, \omega_y, \omega_z]^T$: Angular Rate

μ_L: Gain Margin

φ_m: Phase Margin

μ_{Δ}: Structured Singular Value

ϖ: Frequency

$\mathcal{H}$: Generic Transfer Function

I: Inertia

m: Mass

M: Torque

T: Thrust

Acronyms/Abbreviations

BE: Braking Engines

BIBO: Bounded-Input Bounded-Output

CoG: Center of Gravity

DM: Descent Module

DoF: Degree of Freedom

E2E: End-to-End

EDL: Entry, Descent and Landing

GNC: Guidance, Navigation and Control

IMU: Inertial Measurement Unit

LFT: Linear Fractional Transformation

LTI: Linear Time Invariant

MIMO: Multi Input Multi Output

PI: Proportional-Integral

PID: Proportional-Integral-Derivative

RDA: Radar Doppler Altimeter

SISO: Single Input Single Output

SSV: Structured Singular Value

T/W: Thrust-to-Weight Ratio

1. Introduction

The Entry, Descent and Landing phase for an autonomous space vehicle toward any extra-terrestrial surface, nowadays, is a complex procedure which involves an important effort in designing and developing engineering systems, which can ensure a safe touchdown and guarantee the success of a mission [1, 2, 3, 4, 5]. These considerations hold in particular for those celestial bodies with a thin (or absent) atmosphere for which a full ballistic landing, exploiting only parachute systems, is not performable. Indeed, when dealing with descent and landing, the trajectory of CoG is strongly coupled with the lander attitude. The problem is noticeably worth of interest when atmospheric drag is negligible or absent. Indeed, drag friction has an attitude stabilizing effect since it tends to reduce the horizontal velocities with a consequential total off-vertical angle stabilization.

Over the last years, many researches were focused in design GNC algorithms for attitude and landing. Concerning the attitude GNC, [6, 7] propose nonlinear sliding mode techniques, [8, 9] provide both optimal and robust classes of nonlinear controllers, [10] designs a linear feedback regulator after a proper state transformation, [11] exploit a gain scheduling strategy, and a design of a fault tolerant sliding mode attitude observer is provided by [12]. On the other hand, the landing GNC design is deeply dealt by [13, 14, 15]. Nevertheless, a fundamental feature of the controlled landing, managed by the GNC sub-system working in closed-loop, is the stability of both rotational and translational kinematics [16]. The stability verification in nominal condition and in the presence of uncertainties represents a critical task which must be taken into account.

This paper proposes a novel procedure for the verification of the lander nominal and robust stability. This approach differs from the methods developed over the last years for the robust stability verification of the nonlinear systems (Integral Quadratic Constraint [17] and Popov [18, 19, 20, 21] methods). Indeed, the presented procedure is based on the linear fractional transformation of the system, as proposed in [22], and the system stability verification by means of μ-Analysis [23, 24], by accounting the nonlinearities in a novel manner. However, the great complexity of the GNC model requires the creation of a simplified model which allows the verification of the stability performance, in both the time and frequency domains. The approach is to decouple the translation plant from the rotational plant in order to create a couple of connected SISO structures. Then, the coupled SISO models can be analysed by exploiting the classic frequency response approach through Bode diagrams and criteria [25].

Among the Solar System Celestial bodies, Mars represents a great challenge in EDL GNC design [26, 27]. Therefore, Mars is assumed the target planet along all the paper, fitting the test case on its physical features (i.e. atmosphere, gravity, etc.).

In the first part of this paper (Section 2) the dynamic equations involved during planetary landing are discussed and simplified. In Section 3, the GNC architecture is described, with associated sensors. In Section 4, a standard methodology for robust stability verification is discussed, including the classical approach in frequency domain given by the Bode criterion and the μ-Analysis and in time domain verification through a 6 DoF Monte Carlo campaign. The methodology is applied in Section 5, where a test case is presented and its results are shown and discussed.

2. Lander Mathematical Model

2.1. Full Dynamics Model

The mathematical model of a descent module can be described by two sets of vectorial differential equations, one for translational motion and the other for the rotational motion, with respect to an inertial reference frame. On the left hand side of each equation, the aerodynamic and propulsion forces and torques are taken into account; on the right hand side, the inertial contributions are accounted for. The equations are as follows:

$$\boldsymbol{T} = m(\dot{\boldsymbol{v}}_{\boldsymbol{L}} + 2\boldsymbol{\omega} \times \boldsymbol{v}_{\boldsymbol{L}} + \boldsymbol{\omega} \times \boldsymbol{\omega} \times \boldsymbol{r}_{\boldsymbol{L}} - \boldsymbol{g}), \qquad (1)$$

$$\boldsymbol{M} = \boldsymbol{I}\dot{\boldsymbol{\omega}}_{\boldsymbol{L}} + \boldsymbol{\omega}_{\boldsymbol{L}} \times \boldsymbol{I}\boldsymbol{\omega}_{\boldsymbol{L}}, \qquad (2)$$

where m and $\boldsymbol{I}$ are the lander mass and the inertia matrix respectively, $\boldsymbol{v}_{\boldsymbol{L}}$ is the lander velocity with respect to an inertial reference frame, $\boldsymbol{\omega} = \boldsymbol{\omega}_{\mathbf{M}} + \boldsymbol{\omega}_{\mathbf{C}}$ is the total angular velocity, taking into account the Mars' angular velocity ($\boldsymbol{\omega}_{\mathbf{M}}$) and the lander angular velocity due to Mars' curvature ($\boldsymbol{\omega}_{\mathbf{C}}$), $\boldsymbol{r}_{\boldsymbol{L}}$ is the vector joining lander CoG and planet centre, $\boldsymbol{\omega}_{\boldsymbol{L}}$ is the lander angular rate in the lander body reference frame and $\boldsymbol{g}$ is the gravity acceleration vector. The state variables are $\boldsymbol{x}, \boldsymbol{v}, \boldsymbol{\gamma}, \boldsymbol{\omega} \in \mathbb{R}^3$, they represent the position, the velocity, the attitude and the angular rate, respectively, in an inertial reference frame. The system is non-linear and MIMO: the inputs are the force ($T \in \mathbb{R}^3$) and the torque ($M \in \mathbb{R}^3$) vectors delivered by the engines and the outputs coincide with the states variables ($\boldsymbol{x}, \boldsymbol{v}, \boldsymbol{\gamma}, \boldsymbol{\omega} \in \mathbb{R}^3$) previously mentioned.

2.2. Simplified Dynamics Model

The purpose is to create a couple of connected SISO LTI systems, in order to separately study the vertical translation and rotation stability. Hence, both loops can be studied with the classical SISO LTI systems methodology. The approach represents only a practical strategy to decouple the translation and rotation parts of GNC algorithm, but the dynamics remains completely coupled. The following simplifications are applied:

- The planet (Mars) is considered flat and not-rotating.
    - When assuming short navigation time horizon, the simplification has not consequences on lander stability analysis.
    - It is assumed $\boldsymbol{\omega_M = 0}$, Coriolis' and centripetal contributions are neglected.
- Two-dimensional dynamics.
    - The dynamics of the second planar rotation axis around Y is equivalent to the one of the first axis because the relevant momentum of inertia is almost the same. The same consideration is applicable for the second horizontal DoF along the Y axis.
    - Neglection of the contribute of the gyroscopic term from Euler's equation.
- Atmospheric drag is neglected.
    - The contribute in forces and torques are negligible with respect to the ones provided by thrusters.
    - Drag has stabilizing effect on attitude and vertical velocity. The assumption drives to a more conservative scenario.
- Lander Mass is kept constant.
    - The amount of propellant needed for landing is a small fraction of the overall DM mass.

When dealing with the first two assumptions, a pseudo-inertial reference frame can be defined (as in Figure 1) centred on the planet surface by freezing the DM CoG projection on ground when the propelled phase starts. The $ZX_{Inertial}$ plane also is parallel to the ZX_{Body} plane. Since the lander has been already de-spun before the controlled phase, this statement is correct throughout the whole landing phase. Under the assumptions of flat and not-rotating planet, when assuming a short time horizon, the rotation of the planet about its own axis is negligible and the reference frame can be considered as an inertial one. Hence, the model for analytical verification is a 3-DoF one (Figure 1) including:

- The horizontal DoF along the X axis.
- The vertical DoF along the Z axis.
- The rotation DoF about the Y axis (described by the off-vertical angle θ and its time derivatives).

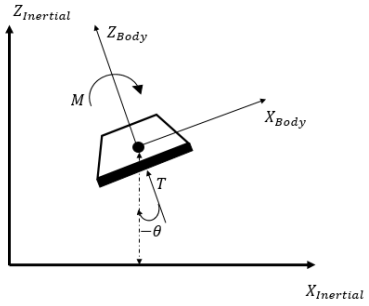

Fig. 1: Dynamics of the Simplified Model for 3-DoF Analysis

Moreover, the rotation about the Z axis (the symmetry axis) is decoupled from the others and not worth of interest for the GNC stability verification. Given the above assumptions, the dynamics equations can be rewritten as follows:

$$\boldsymbol{T} = m(\dot{\boldsymbol{v}}_{\boldsymbol{L}} - \boldsymbol{g}) \,, \qquad (3)$$

$$M = I_y \ddot{\theta} \,. \qquad (4)$$

The simplified model consists in a closed-loop system with the architecture shown in Figure 2. Starting from the initial conditions, the navigation module provides the estimated values of kinematic variables. The guidance segment receives the estimated values as input and provides the reference values feeding the controller. Thus, the control command feeds the BE, which delivers forces and torques to the plant. The loop is also closed by the navigation block that reconstructs the state vector from the measured kinematic quantities. The navigation module feeds also the guidance, which generates the reference profiles by exploiting the navigation measurements.

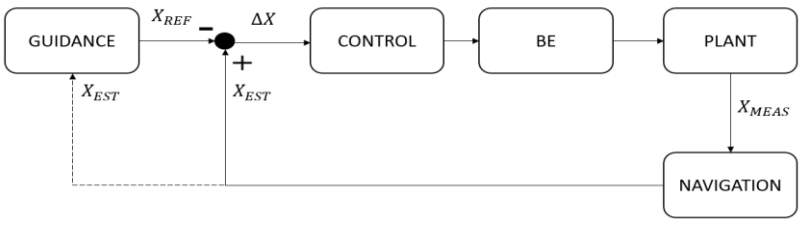

Fig. 2: Simplified Model Architecture

In this diagram the variables X_{REF}, X_{MEAS}, and X_{EST} may be identified as: $X_{REF} = [\bar{\theta},\ \bar{v}_z]$, $X_{MEAS} = [\theta, v_z]$, and $X_{EST} = [\hat{\theta}, \hat{v}_z]$. Note that, the guidance does not compute a reference profile for the horizontal velocity. Nevertheless, the estimated horizontal velocity is used for the computation of the reference attitude profile.

3. GNC Architecture

The landing phase is organized and divided in different sub-phases in order to perform a sort of gains/poles scheduling. During the landing mode, the GNC must be able to adapt its features in order to satisfy different constraints based on guidance policy. The duration of landing phase with activated thrusters is in the order of $25\ s$.

3.1. Navigation Module

The navigation filter aims to determine the state of the system to be controlled. The filter works at $100\ Hz$ in the rotation loop and at $20\ Hz$ in translation loop, being the fastest segment of GNC sub-system, since it must process the RDA and IMU measurements and ensure their prediction. Figure 3 describes in general how the navigation filter works.

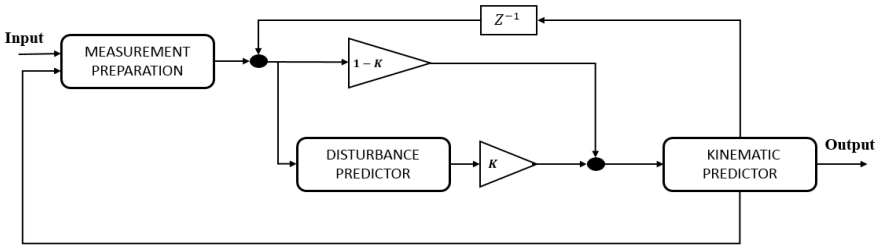

Fig. 3: Schematic Architecture of the Navigation Module

The filter is made up by a kinematic predictor and a disturbance predictor. Indeed, with respect to classical observer structures, a disturbance predictor has been introduced. This approach admits non-stationary disturbance dynamics and the assumptions on the noise statistics are not required. Moreover, the horizontal and vertical navigation modules are provided with a function for pole shift during the propelled phase. The modification of the poles allows the optimization of the performances based on guidance policy.

3.1.1. Kinematic Predictor

Let us assume the classical prediction-correction approach, for a discrete-time system, described by the following set of equations.

$$\boldsymbol{x_{p_{i+1}}} = \boldsymbol{A\hat{x}_i} + \boldsymbol{Bu_i}\,, \qquad (5)$$

$$\boldsymbol{\hat{y}_i} = \boldsymbol{C\hat{x}_i} + \boldsymbol{Du_i}\,, \qquad (6)$$

$$\boldsymbol{\hat{x}_{i+1}} = \boldsymbol{x_{p_{i+1}}} + \boldsymbol{G}\left(\boldsymbol{y_{m_i}} - \boldsymbol{\hat{y}_i}\right), \qquad (7)$$

where $\boldsymbol{\hat{x}}$ is the estimated state vector, $\boldsymbol{x_p}$ is the predicted state vector, $\boldsymbol{y_m}$ is the measurement vector and $\boldsymbol{\hat{y}}$ is the expected measurement vector based on the estimated states. We must take into account the influences, on the states, of the discrepancies between new measurements and expected measurements. The relationship is defined by matrix $\boldsymbol{C}$. The relationship between measurement errors and states is defined through the gain matrix $\boldsymbol{G}$. The correction process takes into account the potential influence of each measurement on the states. The combination of these equations drives to a formulation in which the fundamental characteristic matrix ($\boldsymbol{A - GC}$) is highlighted, whose eigenvalues are chosen such to ensure the stability of the navigation module and the asymptotically convergence of estimation error:

$$\boldsymbol{\hat{x}_{i+1}} = (\boldsymbol{A - GC})\boldsymbol{\hat{x}_i} + \boldsymbol{Bu_i} + \boldsymbol{Gy_{m_i}}\,. \qquad (8)$$

3.1.2. Disturbance Predictor

The disturbance predictor has a structure similar to a kinematic predictor but it works on the residuals of the kinematic predictor process, and hence on the error on the measurement innovation. The states of this process may be considered as the errors on the states of the former process. The combination of the disturbance and kinematic predictors works accordingly to the following transfer function $\mathcal{H}_{Pred}$, from the new measurement to the state estimation:

$$\mathcal{H}_{Pred} = \frac{1-KS}{1+W(1-KS)}\,, \qquad (9)$$

where:

- W is the open loop function of the kinematic predictor.
- K is the fusion gain, mixing a-priori innovation with the filtered contribution in the a-posteriori innovation.

- S is the sensitivity function of the disturbance predictor.

3.2. Guidance Module

The guidance module task is to generate, with a frequency of $10\ Hz$, a reference profile for the control loop based on the measurements estimated by the navigation filter. The vertical translation guidance follows different profiles, depending on each landing phase. In this paper, we consider throttable engines for control, offering the opportunity to change the T/W in a proper larger range between 0 and 3. During the avoidance maneuver, the guidance imposes the vertical velocity kept almost constant by achieving $T/W \approx 1$. The second landing phase aims to strongly reduce the vertical velocity, in order to achieve the minimum speed necessary to perform a safe landing. During this full braking maneuver, the engines provide a T/W between 2 and 3. Nevertheless, in the very last phase of the landing, the thrust profile is smoothly reduced until it reaches a T/W close to 1 with a bounded vertical velocity when the module is close to the ground. The tasks of rotation guidance also depend on the relevant descent profile activated in the landing phase. Indeed, during the back-shell avoidance, the guidance is programmed to sensibly reduce the horizontal velocity through a sudden attitude change. Following this logic, the back-shell moves orthogonally with respect to the descent vehicle following its inertial path. During the full braking phase, the attitude is smoothly verticalized in order to touch the surface with a small off-vertical angle.

3.3. Control Module

The main task of the control module is to provide the command to the thrusters in order to track the guidance kinematic profiles, working at $10\ Hz$. The vertical translation controller is a PI controller and the attitude controller is a PID regulator. The gains are not constant throughout the landing phase, but they change on the basis of the different constraints to be achieved during the landing.

In the paper, the engines mathematical model and description is skipped since it does not influence the overall stability of the model. Nevertheless, few notes on its functionality are mandatory for the comprehension of the control scheme. Briefly, the vertical translation and attitude control loops provide to the thrusters two different commands, related to the necessary thrust to track the reference guidance. In fact, the vertical translation control selects the overall thrust level supplied by the thrusters, allowing the reference vertical velocity tracking. Then, the command from attitude control splits the overall thrust among the engines nozzles, in order to produce a proper torque for attitude stabilization.

3.4 Sensors

In a real EDL system, the sensors for attitude, velocity and altitude determination must be accounted for, in order to provide to the navigation segment the measurements to be processed. A classical choice in EDL design expects the usage of RDA and IMU for a complete set of state variables measurements. In this section, a brief description of the sensors is given in order to better clarify the subsequent discussion on uncertainties for robust stability. Notice that, in our GNC simplified simulator, the RDA and IMU are not present. Nevertheless, their functionalities are accounted for.

3.4.1 Radar Doppler Altimeter

Based on the heritages of a previous Mars landing mission [28], the functionalities of a four-beams pulsed RDA (one central and three lateral 120° apart each other), working at $20\ Hz$, are hereafter described. The minimum number of beams used for computation must be three. With this configuration the oldest datum is two samples older (i.e. $100\ ms$) than the most recent datum in the combination. A further combination with four beams can foresee a delay of $150\ ms$, since the oldest datum is three samples old. Such delays are compensated, through the IMU-provided angular rates and accelerations, and included within the already described navigations tasks.

3.4.2 Inertial Measurement Unit

The IMU is made up by accelerometers for linear kinematics variables determination and gyroscopes for angular rate measurement. In a real EDL sub-system, two differently oriented IMUs are employed, working at $100\ Hz$. Within a simplified GNC simulator, data fusion between the different measurements of two IMUs is managed and processed.

4. Methodology for Robust Stability Verification

In this section, a methodology for robust stability verification is proposed. In general, a feedback control system must ensure the closed loop stability with a sufficient level of robustness, an effective disturbance rejection and a fast set-point tracking. The transfer function of the rotation loop is:

$$\mathcal{H}_{Rot}(z) = \hat{\theta}(z)/\bar{\theta}(z). \qquad (10)$$

The transfer function of the vertical translation loop is:

$$\mathcal{H}_{Des}(z) = \hat{v}_z(z)/\bar{v}_z(z)\ , \qquad (11)$$

where the estimated values ($\hat{\theta}$ and $\hat{v}_z$) are the outcomes of navigation segment and the reference values ($\bar{\theta}$ and $\bar{v}_z$) are the ones provided by the guidance block.

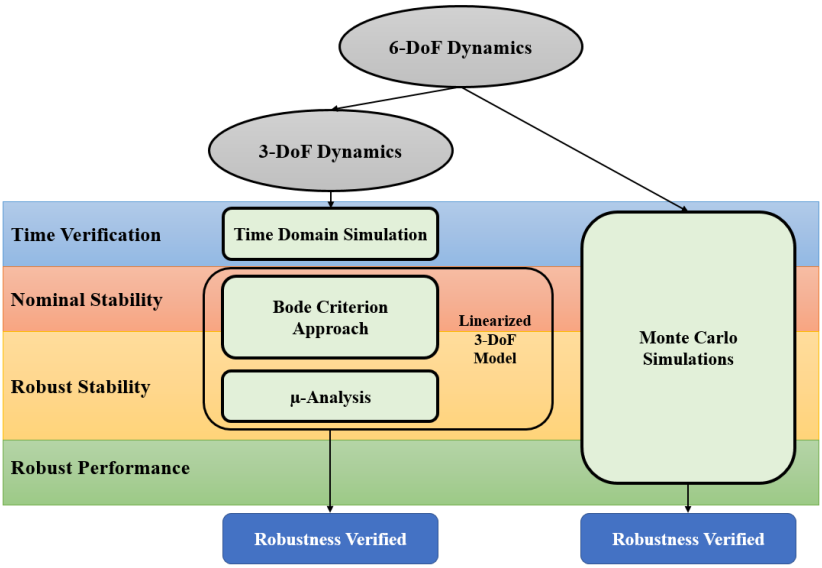

Fig. 4: Methodology for Stability Verification

In Figure 4, the flow chart of the proposed methodology is shown, following two different approaches: an analytical one (on the left branch) and an empirical one represented by Monte Carlo simulations. Indeed, the Monte Carlo campaign has a twofold purpose: the verification of the results out-coming from analytical procedure and the robust performance verification of the system. Indeed, if the time histories of the Monte Carlo campaign do not show any inchoate instability, the final values of state variables at touch-down may be outside any reasonable boundaries, so that no safe landing is performable. Thus, the Monte Carlo campaign is also aimed to verify the robustness of performances by evaluating the reasonability of the values of the controlled variables at touch-down. On the other hand, the analytical methodology can ensure stability of the system (at least local) in a rigorous way, not based on the stochastic behaviour of the Monte Carlo simulations.

4.1. Bode Criterion

A strictly proper discrete-time open-loop transfer function is considered, and it is assumed that the open-loop frequency response has only a single critical frequency ϖ_c and a single gain crossover frequency ϖ_g. Moreover, the open-loop transfer function does not have poles outside the unit circle of the Argand plane. The Bode Criterion ensures the asymptotic stability of the closed-loop if and only if the gain margin μ_L and the phase margin φ_m are both positive. For robustness reasons, the following gain and phase margins must be ensured: $\mu_L > 6\ dB$ and $\varphi_m > 30°$, respectively. This latter is a standard criterion, see, e.g., [29, 30].

4.1.1. Bode Analysis with Variable Delays

The delays in the plant should not affect the stability of this system and the control law should ensure the required performance in the complete range of variations. In presence of uncertainties and delays, the system should still satisfy the Bode Criterion. The approach is the classical one based on Bode plot and criterion and the results will be a set of Bode diagrams.

Engines Action Delay: two different scenarios are considered in order to model different levels of delays: $50ms$ and $60ms$. The thrusters delay is modelled through the Padè approximation [31]. The Padè approximation of a time delay is obtained by means of a Taylor series expansion, as described in [32]. The rational function expressing the Padè approximation of order (m, n) of $e^{-\tau s}$ in the frequency domain is:

$$P_{n,m}(\tau, s) = \frac{q_0+q_1(\tau s)+ \dots +q_m(\tau s)^m}{p_0+p_1(\tau s)+ \dots +p_n(\tau s)^n}, m \leq n \qquad (12)$$

where $P_{n,m}(\tau, s)$ is the transfer function for the Padè delay model and q_m and p_n the relevant coefficients. In the analysis, a symmetrical Padè approximation is chosen (i.e. $m = n$), such that $q_i = (-1)^i p_i, \in \{0, 1, 2, \dots, n\}$, where

$$p_i = \frac{(2n-i)!n!}{(2n)!(n-i)!i!}, i \in \{0, 1, 2, \dots, n\}. \qquad (13)$$

RDA Measurement Delay: the system should be stable also in presence of the delay of the RDA measurements. Indeed, the RDA provides measurements which are a fusion of data collected in the past. Generally, the result of data processing has an average delay that can be larger than $100ms$. However, the navigation algorithm is also able to compensate most of this delay effect through the anticipation of the translation states gathered by the accelerometers.

Therefore, a study of effect of the RDA measurement delay can be tackled by considering values equivalent to the average age of the last, of the older and of the second older samples (i.e. $30ms$, $80ms$ and $130ms$).

4.1.2. Resonance Rejection Analysis

In order to guarantee the simplified SISO system stability with respect to system critical frequency, a resonance rejection analysis is carried out, based on a list of frequency and modal effective mass associated to the first vibration mode. The analysis is important since it allows to exclude that possible undesirable vibration modes affect the GNC loop driving the state variables to divergence. Those critical frequencies must be much higher than the cut-off frequencies of global system. Then, the GNC must reject the first vibration mode frequency, guaranteeing at least $20\ dB$ of margin on Bode diagram.

4.2. μ-Analysis

In Section 2.2. the non-linear dynamics model has been simplified in order to exploit the classical linear tools for stability verification. Nevertheless, from the robust stability points of view, such nonlinear contributions cannot be neglected, since their effects may drive the system outside the linearization domain. Over the last decades, several methods for robust analysis of non-linear systems were developed, such as the Popov criterion [18, 19, 20] and the Integral Quadratic Constraints (IQC) [17]. Even though such methods are extremely powerful, they may need a considerable computational time effort [33]. In this paper, a novel simplified method for μ-Analysis is proposed, able to account for the non-linearities present in a physical plant.

The uncertainties affecting the plant may be grouped into two main classes:

- Parametric uncertainties: real or complex are due to a non-precise knowledge of the system parameters.
- Uncertainties due to neglected dynamics: due to a lack of knowledge or a simplification of the physical behavior of the system of interest.

By introducing the LFT formalism [22], the uncertainties matrix $\Delta(s)$ is connected to a given system $\boldsymbol{M}(s)$, as represented in Figure 5. In the case of LTI systems, the different perturbations are lumped in a unique perturbed system. In our case $\Delta_i(s) = \delta_i \boldsymbol{I}$ is a time invariant diagonal matrix, where δ_i denotes a real of complex structured uncertainty or, in the case of neglected dynamics, a proper, stable and rational transfer function. We introduce the notation $\Delta(s) \in \boldsymbol{\Delta}$, where $\boldsymbol{\Delta}$ accounts all the variations of Δ for the whole frequency range of interest. Then, introducing the largest singular value $\bar{\sigma}$, a normalized set of structured uncertainty is defined as follows:

$$\boldsymbol{B_{\Delta}} = \{\Delta \in \boldsymbol{\Delta} : \bar{\sigma}(\Delta) < 1\}\,. \qquad (14)$$

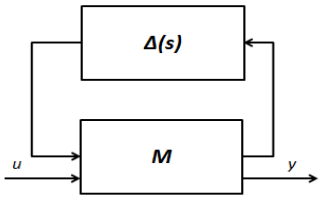

Fig. 5: Standard $\boldsymbol{M}-\boldsymbol{\Delta}$ Configuration

Therefore, the uncertainties set has the following structure:

$$\boldsymbol{\Delta} = \{diag[\delta_1 \boldsymbol{I}_{s1}, \dots, \delta_r \boldsymbol{I}_{sr},\ \varphi_1 \boldsymbol{I}_{s1}, \dots, \varphi_c \boldsymbol{I}_{sc},\ \Delta_1, \dots, \Delta_F]\colon \delta_i \in \mathbb{R}, \varphi_i \in \mathbb{C}, \Delta_j \in \mathbb{C}^{m_j \times m_j}\}\,. \qquad (15)$$

The feedback connection $F(\boldsymbol{M}, \boldsymbol{\Delta})$ is stable if and only if, at each given frequency ϖ:

$$\sup_{\varpi \in \mathbb{R}} \left(\mu_{\boldsymbol{\Delta}}\big(\boldsymbol{M}(j\varpi)\big) \leq 1\right), \qquad (16)$$

where $\mu_{\boldsymbol{\Delta}}$ is the structured singular value as in equation *(17)*:

$$\mu_{\boldsymbol{\Delta}}(\boldsymbol{M})^{-1} = \inf_{\Delta \in \boldsymbol{\Delta}} \{\|\Delta\| : \det(\boldsymbol{I} - \boldsymbol{M}\Delta) = 0\}. \qquad (17)$$

In general, the computation of the margin introduced in *(16)* and *(17)* cannot be tackled analytically. A more comfortable way of accomplishing μ-Analysis is to find the upper and lower margins of structured singular value. Nevertheless, also computing these bounds may be a challenging problem as showed in [34] where numerical approximate methods for μ margins computation are provided. The analysis carried out in this paper is based on the numerical procedure described in [34] and [35].

Remark. μ-Analysis guarantees robust stability of the closed-loop linearized system, which implies local robust stability of the closed-loop nonlinear system. This is not sufficient to guarantee that the nonlinear system has bounded state and output signals for all possible disturbance and reference signals. Nevertheless, local robust stability is important to avoid that arbitrarily small disturbance or reference signals make the nonlinear system diverge. In other words, robust

stability of the linearized system can be seen as a sort of necessary (but not sufficient) condition for having bounded solutions of the nonlinear system, in the presence of not too large disturbances.

Remark. The above formulation of μ-Analysis and subsequent considerations are standard. The topics presented in the following are not standard. They are developed ad hoc for planetary landing problems and, to the best of our knowledge, they represent a novel contribution beyond the state of the art.

4.2.1. Structured Uncertainties

The following structured uncertainties are taken into account for the μ-Analysis:

- Mass and Inertia Uncertainties: The mass uncertainty is computed as the difference between the initial and final mass of the vehicle at each landing mode considered. As far as inertia uncertainty, it is larger due to the error introduced by the inertia measurement instrumentation. It is estimated as the mass uncertainty plus 1%.
- Force and Torque Uncertainties: the thrusters uncertainty may be addressed to the harmonic pulsation in the combustion chamber. For the sake of conservativeness, the thrusters uncertainties are declared constant.
- Angular Uncertainty: The error allocation has been performed based on the gyroscopes bias stability over 3σ, where σ is the standard deviation, discussed in [36].
- Slant and Doppler Velocity Uncertainties: The uncertainties for the Doppler velocity and the slant range are estimated on the basis of [28].

4.2.2. Neglected Dynamics

The nonlinear dynamics of a landing spacecraft is treated as neglected dynamics. Indeed, a non-linear system can be seen as a linear plant connected in feedback with a nonlinear block (Figure 6).

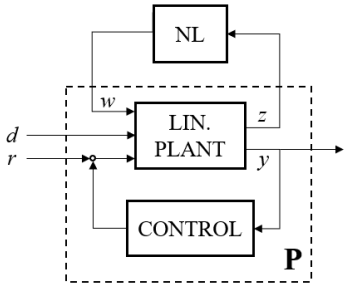

Fig. 6: Linear Plant with Non-linear Contributions

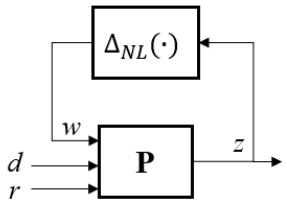

Fig. 7: Linear Plant with Non-linear Uncertainties

In the figure, $d(t) \in S_D$ is a bounded disturbance and $r(t) \in S_R$ is a bounded reference signal, with $S_D, S_R \subset \mathbb{R}^n$. By recalling the LFT notation, the above system may be recasted in the form of Figure 7, where Δ_{NL} is a static function collecting all the involved nonlinearities. A cut-off frequency is identified in order to neglect nonlinear effects at very high frequencies. The model is sampled at $100\ Hz$, in order to fulfill the Nyquist-Shannon theorem. Then, a simple pole is placed at $20\ Hz$. Such a value is large enough not to reject resonance phenomena coming from the GNC loop. The input-output gain of Δ_{NL} is evaluated as a suitable induced norm of the non-linear uncertainty, by opening the loop as in Figure 8 and injecting the contributions given by the linear plant.

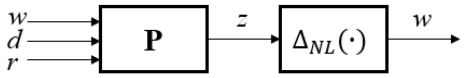

Fig. 8: Linear Plant with Non-linear Uncertainties Open-loop

Considering the signals in Figure 8, the induced norm is defined as follows:

$$\|\Delta_{\mathrm{NL}}\|_\infty = \sup_{z \neq 0} \frac{\|w\|_\infty}{\|z\|_\infty} \ . \qquad (18)$$

The non-linearities accounted in Δ_{NL} are the Coriolis and centripetal accelerations in the Newton's law (taking into account the Mars' rotation angular velocity) and the gyroscopic term in the Euler's equation. Moreover, the controlled thrust must be projected along the z-axis of inertial reference frame, introducing a non-linear term equal to $T cos\theta$ within the vertical translation dynamics equation. Then, the Δ_{NL} infinity norm is computed numerically by exploring the whole domains of S_D and S_R.

Let us now characterize the disturbance signals. The main a-priori hypothesis concerns the bounds of their variation domain. In this paper, two different kinds of perturbations are taken into account:

- Perturbation of dispatched forced and torques

- Perturbations due to wind gust.

The last perturbation type is supposed to affect both the angular and linear velocities. Then, although the lander has been already de-spun, this hypothesis allows not to nullify the gyroscopic torques, $\omega_x\omega_z(I_x - I_z)/I_y$ and $\omega_y\omega_z(I_z - I_y)/I_x$, depending on ω_z, which is nominally null. The vertical and horizontal gusts are modelled as random uniform (bounded) signals, affecting vertical and horizontal velocities and spinning and transversal angular rates.

Concerning the disturbances outcoming from the thrusters, they are modelled as a sinusoidal signal with a bounded amplitude with a frequency of $1\,Hz$. This choice is aimed to represent the fluctuating pressure within the combustion chamber due to an unperfect combustion of the propellant.

4.3. Monte Carlo Analysis

The purpose of the Monte Carlo analysis is to complete the overall stability verification process, in order to verify the reliability of the methodology depicted in previous sections. The analysis is performed through a 6 DoF E2E simulator which takes into account the full dynamics and the full modeling of the sensors involved in the landing architecture. Moreover, the Monte Carlo simulations allow to verify, empirically, the system robust performance, that could have been also verified through the theoretical μ procedure.

Indeed, the campaign allows to study the 6 DoF kinematics in the presence of randomized uncertainties on input parameters. In the case, the verification of possible inchoate instability is a critical task which shall confirm the results coming from the Bode diagrams and μ-Analysis.

Remark. If a linear parameter varying (LPV) or gain-scheduling controller is used, it may happen that the change of controller parameters destabilizes the closed-loop system. A huge number of applications can be found in the aerospace field where this problem arises. However, the theoretical stability verification in the presence of time-varying parameters is difficult from a mathematical point of view. Monte Carlo simulations are typically used to perform a “numerical” stability verification. In this paper, we follow such an approach.

5. Test Case

Now, the methodology is applied to a real test case representing a descent module achieving a planetary soft landing. Mars is the target planet for the test case. Therefore, focusing the attention on the landing propelled phase, three different phases are identified, each one with different goals to be achieved. In summary, during the first phase, the aim is to let the back-shell to turn away from the landing vehicle, keeping the T/W equal to unit value. In second phase, engines provide more thrust as possible in order to sudden reduce the vertical velocity. In the last phase, T/W reduces again in order to perform a safe soft landing.

Let us now define the mass and inertia configuration for test case. Such values are based on the heritage of heavy Mars lander designs [26, 27].

Mass $[kg]$	Inertia I_{yy} $[kgm^3]$	Thrust Range $[kN]$
1220	1030	$0 \div 13$

Table 1: Summary of Lander Configuration Parameters

The initial conditions for the different three phases are listed in Table 2. The phase switching is automatically managed by the guidance, on the basis of the estimated altitude and vertical velocity values. Note that, the last phase is stopped (and the braking engines are switched-off) when the first one of the landing appendages, used by the descent module to lean on the terrain, touches the Martian surface. This condition is hard to be implemented in a simplified simulator: an altitude of 1.5 m is imposed as switching-off condition. This value is a reasonable choice which accounts the lander CoG distance from the appendage extremity, the terrain slope and the attitude at the touchdown. Finally, the control gains (which are the worthiest of interest GNC parameters) are listed in Table 3.

	PHASE 1	PHASE 2	PHASE 2
Altitude [m]	595.90	195.42	16.24
Vertical Velocity $[m/s]$	37.97	34.43	7.07
Off-vertical Angle $[rad]$	0.1905	-0.0021	-0.0026
Angular Rate $[rad/s]$	0.0140	-0.0174	-0.0054

Table 2: State Variables Initial Conditions of the Descent Phases for a reference landing realization

	CONTROL GAINS	PHASE 1	PHASE 2	PHASE 3
Vertical Translation Control	K_P	10	20	40
	K_I	0.5	0.5	0.5
Attitude Control	K_P	2	1	1
	K_I	0.25	0.25	0.25
	K_D	6	3	3

Table 3: Control Gains

5.1. Time Domain Verification

This subsection is dedicated to verify the consistency of the linearized system with respect to the complete one as introduced in Section 2.2. for the considered test case. The profile of kinematics, the control actions, the estimate values of the state vector, with respect to the reference profiles as well, can be observed for the overall landing period. The evaluation of time-histories allows a preliminary observation and a first level of assessment of each physical state, as well as of the coherence of the estimated values with the reference ones. Note that, small jittering behavior (Figure 9 and Figure 10) may be due to the transition between two different phases, where sudden changes of reference profiles occur.

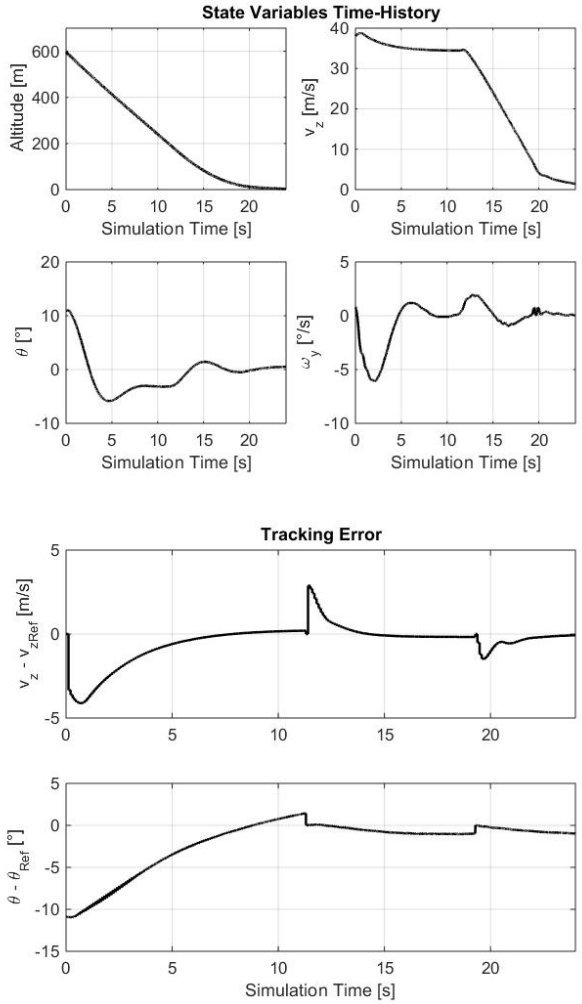

Fig. 9: State Variables Time-History and Output Tracking Error

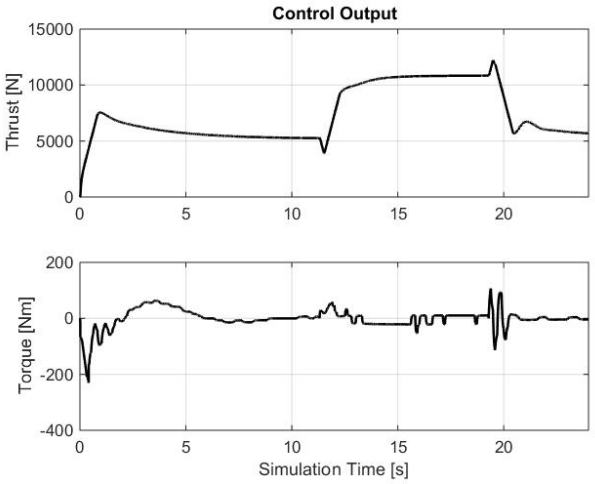

Fig. 10: Force and Torque Time-History

The figures above show the consistency of the results with the aims of GNC in the landing phases previously described. Indeed, a first remark can be addressed to thrust profile which is perfectly in line with the T/W requirements sketched in previous sections.

5.2. Bode Criterion Verification

Bode open-loop diagrams where extrapolated by linearizing the loops, in order to extract the values of gain and phase margins for nominal stability.

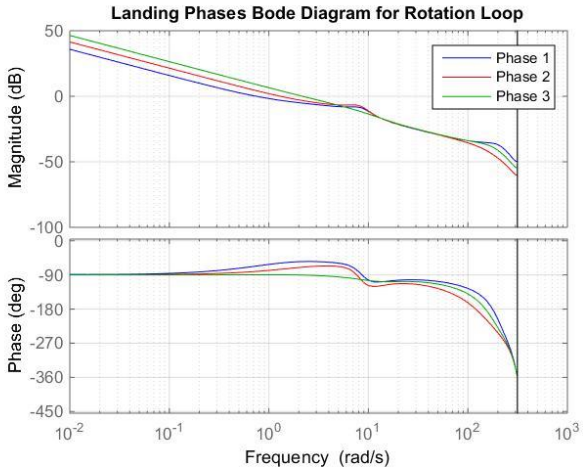

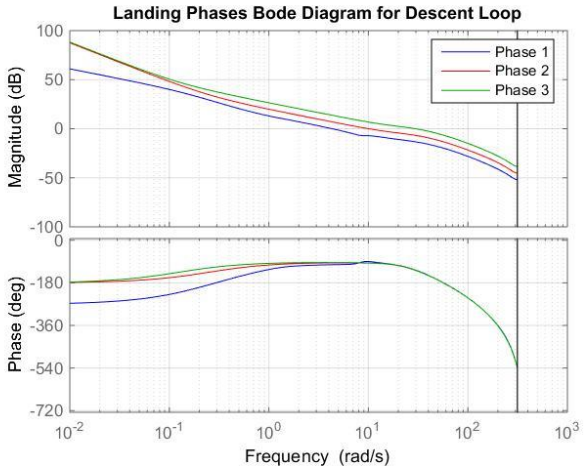

Fig. 11: Bode Diagrams of Landing Phases

In Table 4, the minimum margins for nominal stability are summarized. Both configurations are widely stable. The system, in all phases, is compliant with the robust margins threshold cited in Section 4.1. (i.e. $\mu_L > 6\ dB$: and $\varphi_m > 30°$).

		Vert. Transl.	**Rotation**
PHASE 1	*Gain Margin [dB]*	19.8	35.8
	Phase Margin [°]	77	114
PHASE 2	*Gain Margin [dB]*	13.2	37.7
	Phase Margin [°]	83.4	105
PHASE 3	*Gain Margin [dB]*	6.47	36.6
	Phase Margin [°]	53.5	89.6

Table 4: Summary of Stability Margins

5.2.1. Bode Verification with Variable Delays

The Bode verification with variable delays is based on the theory explained in Section 4.1.1. The margins are picked only during the landing Phase 2. Indeed, in that phase, the thrusters provide the maximum thrust (force and torque) possible, thus, the study on its delays, in that landing mode, is worthier of interest.

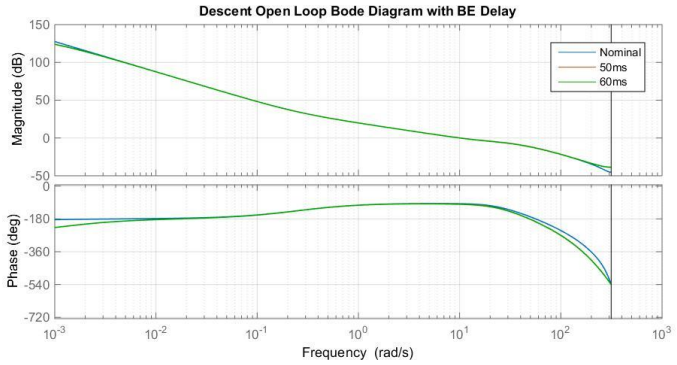

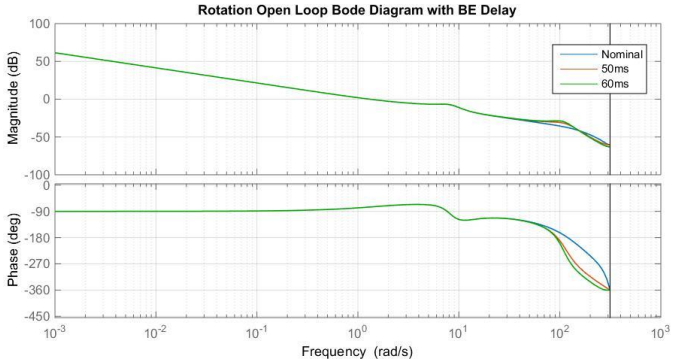

Fig. 12: Landing Phase 2: Bode Diagrams with Engines Delays

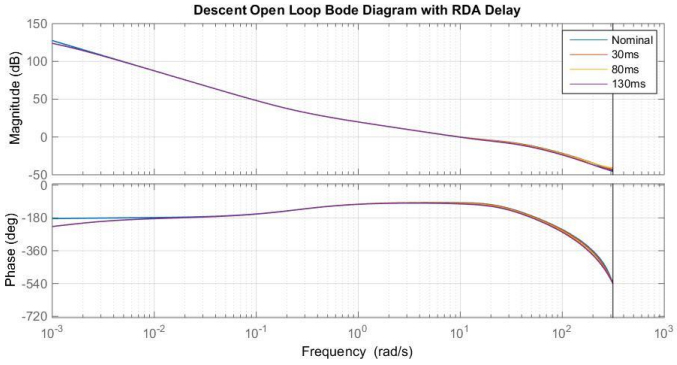

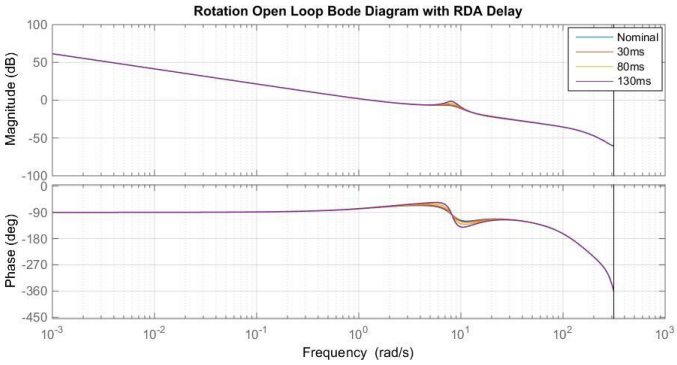

Fig. 13: Landing Phase 2: Bode Diagrams with RDA Delays

Delays and uncertainties, applied to the GNC loops, does not affect widely the system stability. The curves are almost overlapped, and the margins variations range is quite narrow. The observations are confirmed by matching the results in Table 5 with the data in Table 4. Therefore, all margins are fully compliant with Bode requirements: both vertical translation and rotation loops are widely stable.

PHASE 2			
	Minimum Margins	**Vert. Transl.**	**Rotation**
Engines Delays	*Gain Margin [dB]*	11.5	28.6
	Phase Margin [°]	80.3	105
RDA Delays	*Gain Margin [dB]*	13.2	37.6
	Phase Margin [°]	77.1	105

Table 5: Summary of Minimum Stability Margins with Delays

5.2.2. Resonance Rejection Verification

From Figure 11 is possible to evaluate the rejection margins relevant to critical frequencies for all landing modes. In the fact, the rotation shall withstand a possible resonance at $13\ Hz$, whilst the vertical translation loop shall withstand a resonance located at $22.5\ Hz$.

		Critical Frequency [Hz]	***Rejection Margin [dB]***
PHASE 1	**Vert. Transl.**	22.5	34.2
	Rotation	13	32.7
PHASE 2	**Vert. Transl.**	22.5	33.6
	Rotation	13	27.7
PHASE 3	**Vert. Transl.**	22.5	32.6
	Rotation	13	21.0

Table 6: Summary of Resonance Rejection Margins

In Section 4.1.2. the minimum threshold for robustness rejection of resonance phenomena was set at $-20\ dB$. Therefore, the system is fully robust versus resonance phenomena.

5.3 μ-Analysis Results

The following figures are representative of the theory and methodology described in Section 4.2. Indeed, for each landing phase the bounds of the SSV are plotted in order to verify that their values never cross the unit threshold. Therefore, the robust stability of the linearized system is fundamental since it can be seen as a sort of necessary (but not sufficient) condition for having bounded solutions of the nonlinear system, in the presence of not too large disturbances. These disturbances account the configuration, sensors, and actuators uncertainties, but mostly the nonlinearities (centrifugal and Coriolis' acceleration, descent/control coupling, and gyroscopic effects) are treated in a novel manner, enforcing the results and the consistency of the μ-Analysis.

The following values of the induced norms have been estimated, numerically, for the three phases:

$$\|\Delta_{DES}\|_\infty = 0.2059\ (phase\ 1),\ 0.4831\ (phase\ 2), 0.4867\ (phase\ 3),$$

$$\|\Delta_{ROT}\|_\infty = 0.0099\ (phase\ 1),\ 0.0110\ (phase\ 2), 0.0118\ (phase\ 3).$$

They represent the magnitude of the nonlinearities accounted for the μ-Analysis and treated as neglected dynamics. By observing the SSV behavior in all landing phase, the system robustness stability is guaranteed.

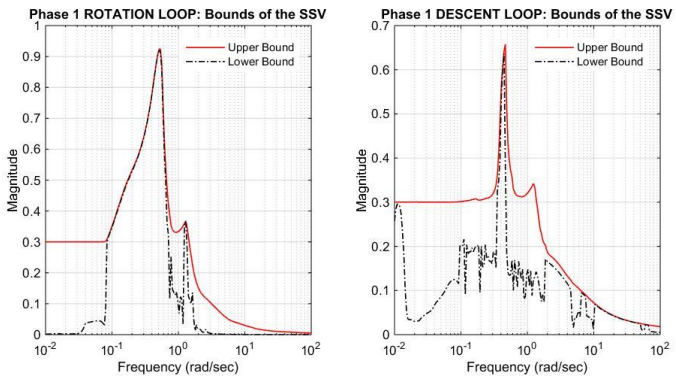

Fig. 14: Landing Phase 1: Bounds of SSV

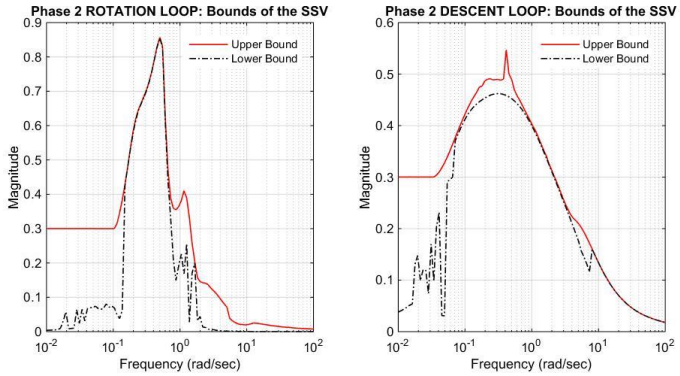

Fig. 15: Landing Phase 2: Bounds of SSV

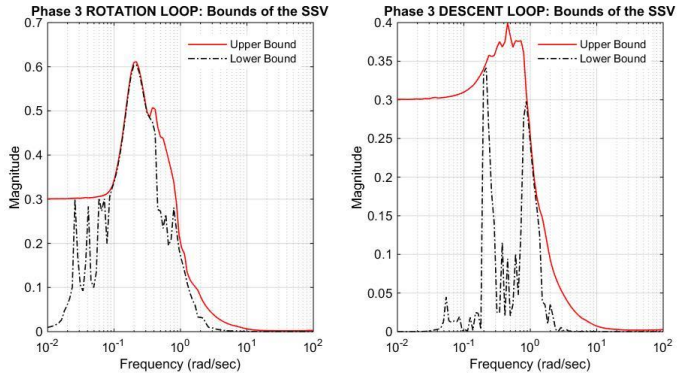

Fig. 16: Landing Phase 3: Bounds of SSV

5.4 Monte Carlo Campaign

Looking at the time histories of the 6-DoF dynamics state variables, it is important to verify that no inchoate instability is noticeable. Moreover, when dealing off-vertical angles and lateral rates in full kinematics, the terminology stands for the overall contribute of angular variable, meant as the Euclidian norm. The remarks explain why in Figure 18 angular values do not assume any negative value.

Therefore, the full robustness stability of landing system is confirmed by Monte Carlo simulations too. In fact, no inchoate instability is present, and the system is kept stable for a large variation of uncertainties.

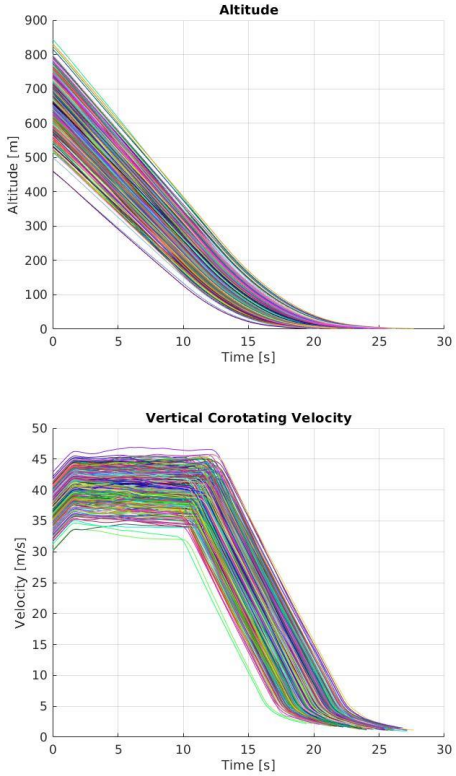

Fig. 17: Time Histories of the Vertical Translation State Variables

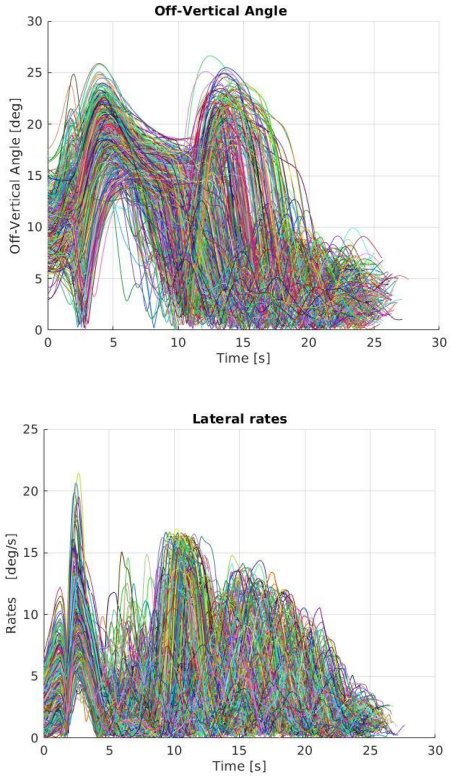

Fig. 18: Time Histories of Rotation State Variables

6. Conclusion

In this paper, a methodology for robust stability assessment related to a complex GNC problem has been presented. The methodology allows, after model simplifications, to study the stability of an autonomous planetary lander exploiting the items relevant the classical control theory framework. Eventually, the evaluation of system behavior was matched with the results of Monte Carlo campaign (performed with an E2E simulator) in order to verify the consistency of stability margins with the time history of state variables in 6 DoF dynamics in presence of random bounded uncertainties.

Moreover, the test cases have been deeply analyzed. The stability of nominal system is ensured through gain and phase margins highlighted by Bode diagrams. The same approach has been exploited in presence of uncertainties and delay in the frame of a preliminary robustness assessment. The Bode plots allow to identify the minimum stability margin during the most stressful landing phase, when the thrusters supply the maximum available thrust. Eventually, μ-Analysis confirmed the goodness of those margins ensuring system robustness stability for each landing phase, in presence of the identified structured uncertainties and system delays. The last step allowed to identify the rejection guaranteed by GNC at the first mode frequencies. Since the resonance frequency is rejected in all cases beneath the prescribed threshold, the system is considered robustly stable. Monte Carlo results in Section 5.4. assessed that the model simplifications did not modify the system stability and confirmed the goodness of the depicted methodology.

Conflict of interest statement

Authors are agreed for the publication of this paper and there is no conflict of interest.

Acknowledgments

We want to thank the whole E2E team from Thales Alenia Space in Turin for the great work in developing the E2E simulator and for the support in our research. In the case, great thanks go to Simona De Sanctis, Ludovico Garin, Fabio Calantropio, Davide Granà and Liliana Torre. We want also to thank the GNC team chief, Andrea M. R. Bacchetta and the Avionics team chief, Mario Montagna, for the precious suggestions and support along paper developing.

References

[1] D. Desiderio, M. Lovera, Guidance and Control for Planetary Landing: Flatness-Based Approach, IEEE Transaction on Control System Technology, 21(4):1280-1294, July 2013. https://doi.org/10.1109/TCST.2012.2202664.

[2] P. Martella, M. Buonocore, D. Desiderio, M. Lovera, S. Portigliotti, Soft landing on Mars: The GNC tasks in the ExoMars descent module mission, Proceedings. 7th Int. ESA Conference of Guidance, Navigation and Control System., pp. 1-13, 2008.

[3] F. Najson, K. Mease, Computationally inexpensive guidance algorithm for fuel-efficient terminal descent, Journal of Guidance and Control Dynamics, vol. 29, no. 4, pp. 955-964, 2006. https://doi.org/10.2514/1.17715.

[4] U. Topcu, J. Casoliva, K. Mease, Minimum-fuel powered descent for Mars pinpoint landing, Journal of Spacecraft Rockets, vol. 44, no. 2, pp. 324-331, 2007. https://doi.org/10.2514/1.25023.

[5] F.J. Arias, S. De Las Heras, Sandbraking. A technique for landing large payloads on Mars using the sands of Phobos, Aerospace Science and Technology 85(2019), 409–415.

[6] P.M. Tiwari, S. Janardhanam, M. un Nabi, Attitude Control Using Higher Order Sliding Mode, Aerospace Science and Technology 54 (2016), 108-113.

[7] A. Sofyali, E.M. Jafarov, R. Wisnieski, Robust and global attitude stabilization of magnetically actuated spacecraft through sliding mode, Aerospace Science and Technology 76(2018), 91–104.

[8] Y. Park, Inverse Optimal and Robust Nonlinear Attitude Control of Rigid Spacecraft, Aerospace Science and Technology 28 (2013), 257-265.

[9] Y. Park, Robust and Optimal Attitude Control of Spacecraft with Inertia Uncertainties Using Minimal Kinematic Parameters, Aerospace Science and Technology 54 (2016), 276-285.

[10] W. Luo, B. Zhou, G.R. Duan, Global stabilization of the linearized three-axis axisymmetric spacecraft attitude control system by bounded linear feedback, Aerospace Science and Technology, 78(2018), 33–42.

[11] R. Jin, X. Chen, Y. Geng, Z. Hou, LPV gain-scheduled attitude control for satellite with time-varying inertia, Aerospace Science and Technology, 80(2018), 424–432.

[12] B. Li, Q. Hu, Y. Yang, Continuous finite-time extended state observer-based fault tolerant control for attitude stabilization, Aerospace Science and Technology 84(2019), 204–213.

[13] L. Shuang, C, Pingyuan, C. Hutao, Autonomous Navigation and Guidance for Landing on Asteroids, Aerospace Science and Technology 10 (2006), 239-247.

[14] L. Shuang, C, Pingyuan, C. Hutao, Vision-aided Inertial Navigation for Pinpoint Planetary Landing, Aerospace Science and Technology 11 (2007), 499-506.

[15] J.W. Jang, L.Yang, M. Fritz, L.H. Nguyen, W.R. Johnson, J.J. Hart, Design and Analysis of Morpheus Landed Flight Control System, AIAA, 2004. https://doi.org/10.2514/6.2014-4115.

[16] P. Martella, M. Buonocore, E. Canuto, A. Molano, R. Drai, L. Lorenzoni, Design and Verification of the GNC for the European ExoMars EDL Demonstrator, AIAA Guidance, Navigation, and Control Conference 08 - 11 August 2011, Portland, Oregon. https://doi.org/10.2514/6.2011-6341.

[17] A. Megretski, A. Rantzer, System Analysis via Integral Quadratic Constraints, IEEE Transaction on Automatic Control, Vol. 42, No. 6, June 1997. https://doi.org/10.1109/9.587335.

[18] V. M. Popov, On Absolute Stability of Non-linear Automatic Control Systems, Avtomat. i Telemekh., 1961, Volume 22, Issue 8, 961–979.

[19] J.P. How, S.R. Hall, Connections between the Popov Stability Criterion and Bounds for Real Parameter Uncertainty, Proceedings of the American Control Conference, San Francisco, California, June 1983. https:// doi.org/10.23919/ACC.1993.4793033.

[20] P.A. Bliman, Extension of Popov Absolute Stability Criterion to Non-autonomous Systems with Delays, International Journal of Control, 73:15, 1349-1361. https://doi.org/10.1080/002071700445370.

[21] S. Fekri, D. Bates, I. Postlethwaite, Linear vs. Nonlinear Robustness Analysis: A Case Study, 16th IEEE International Conference of Control Application, Singapore, 1-3 October 2007. https://doi.org/10.1109/CCA.2007.4389323.

[22] J. Doyle, Analysis of feedback systems with structured uncertainties, IEE Proceedings, Part D, vol. 129, no. 6, pp. 242-250, 1982. https://doi.org/10.1049/ip-d.1982.0053.

[23] A. Marcos, J.M. Biannic, M. Jeanneau, D. Bates, I. Postlethwaite, Aircraft Modelling for Nonlinear and Robust Control Design and Analysis, IFAC Proceedings, Volume 39, Issue 9, 2006, 679-684. https://doi.org/10.3182/20060705-3-FR-2907.00116.

[24] A. Iannelli, P. Simplicio, D. Navarro-Tapia, A. Marcos, LFT Modeling and μ Analysis of the Aircraft Landing Benchmark, The International Federation of Automatic Control, 20th Congress, Tolouse, France, July 9-14, 2017. https://doi.org/10.1016/j.ifacol.2017.08.766.

[25] P. Martella, S. De Sanctis, D. Granà, A. Amelio, D. Temperanza, A. Martinez Barrio, The Verification Approach of The ExoMars EDM GNC, Proceedings of 9th International ESA Conference on Guidance, Navigation & Control Systems, June 2014, Oporto, Portugal.

[26] D.W. Way, R.W. Powell, A. Chen, A. D. Steltzner, A.M. San Martin, P.D. Burkhart, G.F. Mendek, Mars Science Laboratory: Entry, Descent, and Landing System Performance, Proceeding of the 2007 IEEE Aerospace Conference, Big Sky, Montana, 2007. https://doi.org/10.1109/AERO.2007.352821.

[27] R.D. Braun, R.M. Manning, Mars Exploration Entry, Descent, and Landing Challenges, Journal of Spacecraft and Rockets, Vol. 44, No. 2, March-April 2007. https://doi.org/10.2514/1.25116.

[28] O. Bombaci, M. Iorio, P. Pepe, Exomars Radar Doppler Altimeter (A Doppler radar for accurate attitude measurements in support to landing phase), Proceeding of the 3rd IEEE International Workshop on Metrology for Aerospace, Florence, Italy, 2016. https://doi.org/10.1109/MetroAeroSpace.2016.7573187.

[29] K.J. Åström, R.M. Murray, Feedback Systems: An Introduction for Scientists and Engineers, Princeton University Press, Princeton, NJ, 2008.

[30] European Space Agency, ECSS-E-ST-60-10C – Control performance, November 2008.

[31] G.H. Golub, C.F. Van Loan, Matrix Computations, Johns Hopkins University Press, Baltimore, 1989, pp. 557-558.

[32] Y. Wei, Y. Hu, Y. Dai, Y. Wang, A generalized Padé approximation of time delay operator, International Journal of Control, Automation and Systems, February 2016, Volume 14, Issue 1, pp 181–187. https://doi.org/10.1007/s12555-013-0240-4.

[33] J. Chaudenson, Robustness analysis with integral quadratic constraints, application to space launchers, Other, Supélec, 2013.

[34] D.W. Gu, P. Hr. Petkov, M. M. Konstantinov, Robust Control Design with MATLAB, Springer, 2005.

[35] P.M. Young, M. P. Newlin, J.C. Doyle, μ-Analysis with Real Parametric Uncertainty, Proceedings of the 30th Conference on Decision and Control, Brighton, England, December 1991. https://doi.org/10.1109/CDC.1991.261579.

[36] G. Cros, Ph. Loubières, I. Lainé, S. Ferrand, Th. Buret, Ph. Guay, European Astrix Fogs In-Orbit Heritage, 8th International ESA Conference on Guidance, Navigation & Control Systems, Karlovy Vary, Czech Republic, 2011.